Journal of Sound and Vibration 330 (2011) 771–787

Contents lists available at ScienceDirect

Journal of Sound and Vibration

journal homepage: www.elsevier.com/locate/jsvi

Analysis of thick isotropic and cross-ply laminated plates by radial basis functions and a Unified Formulation

A.J.M. Ferreira [a,*], C.M.C. Roque [b], E. Carrera [c], M. Cinefra [c]

[a] Departamento de Engenharia Mecânica, Faculdade de Engenharia da Universidade do Porto, Rua Dr. Roberto Frias, 4200-465 Porto, Portugal
[b] INEGI, Faculdade de Engenharia da, Universidade do Porto, Rua Dr. Roberto Frias, 4200-465 Porto, Portugal
[c] Department of Aeronautics and Aerospace Engineering, Politecnico di Torino, Corso Duca degli Abruzzi, 24, 10129 Torino, Italy

ARTICLE INFO

Article history:
Received 29 May 2010
Received in revised form
25 August 2010
Accepted 26 August 2010
Handling Editor: S. Ilanko
Available online 15 September 2010

ABSTRACT

In this paper, we combine Carrera's Unified Formulation and a radial basis function collocation technique for predicting the static deformations and free vibration behavior of thin and thick isotropic and cross-ply laminated plates. Through numerical experiments, the capability and efficiency of this collocation technique for static and vibration problems are demonstrated, and the numerical accuracy and convergence are thoughtfully examined.

1. Introduction

The Unified Formulation (UF) proposed by Carrera [1–5] is a powerful framework for the analysis of beams, plates and shells. This formulation has been applied in several finite element analysis, either using the Principle of Virtual Displacements or by using Reissner's Mixed Variational theorem. The stiffness matrix components, the external force terms or the inertia terms can be obtained directly with this UF, irrespective of the shear deformation theory being considered.

In this paper, for the first time, we propose to use this UF to derive the equations of motion and boundary conditions to analyze isotropic and cross-ply laminated plates by radial basis functions (RBF) collocation. We consider as examples two shear deformation theories *for which the UF generates the discretized set of collocation equations with the same basic approach and coding*. We consider here a first-order shear deformation theory (FSDT), disregarding the normal transverse stress σ_z, and the higher-order theory (HSDT) of Kant [6,7] considering non-zero normal shear deformation ε_z.

The combination of the UF and collocation with RBFs provides an easy, highly accurate framework for the solution for plates, under any kind of shear deformation theory, irrespective of the geometry, loads or boundary conditions. In this sense, this can be considered a generalized RBF formulation.

The analysis of thin and moderately thick plates has been modeled by thin-plate theories, or by shear deformation theories. Typically, such theories involve a constant transverse displacement across the thickness direction, making the transverse normal strain and stress negligible. This assumption is adequate for thin-plates or plates for which the thickness-to-ratio h/a is smaller than 0.1. For higher h/a ratios, the use of shear deformation theories considering the contribution of the transverse normal strain and stress is fundamental. Among such theories, the pioneering higher-order plate theory of Lo et al. [8,9] is attractive due to its simplicity and implementation in a computer code. The higher-order transverse and normal plate theory of Kant and colleagues [6,7] consider not only a cubic evolution of the in-plane displacements with the thickness direction (z), but also a parabolic evolution of the transverse displacement with z.

* Corresponding author.
E-mail address: ferreira@fe.up.pt (A.J.M. Ferreira).

0022-460X/$ - see front matter © 2010 Elsevier Ltd. All rights reserved.
doi:10.1016/j.jsv.2010.08.037

The theory was successfully implemented by finite elements or analytical solutions [6,7,10]. Recently the work of Batra [11] and Carrera [1–3] show interesting ways of computing transverse and normal stresses in laminated composite or sandwich plates. Higher-order theories in the thickness direction were also addressed by Librescu et al. [12], Reddy [13] and more recently by Fiedler and colleagues [14] who considered polynomial expansions in the thickness direction. None of such approaches considered the modeling by radial basis functions.

Recently, radial basis functions (RBFs) have enjoyed considerable success and research as a technique for interpolating data and functions. A radial basis function, $\phi(\|x-x_j\|)$ is a spline that depends on the Euclidian distance between distinct data centers x_j, $j=1,2,\ldots,N \in \mathbb{R}^n$, also called nodal or collocation points. Although most work to date on RBFs relates to scattered data approximation and in general to interpolation theory, there has recently been an increased interest in their use for solving partial differential equations (PDEs). This approach, which approximates the whole solution of the PDE directly using RBFs, is truly a mesh-free technique. Kansa [15] introduced the concept of solving PDEs by an unsymmetric RBF collocation method based upon the MQ interpolation functions, in which the shape parameter may vary across the problem domain.

The analysis of plates by finite element methods is now fully established. The use of alternative methods such as the meshless methods based on radial basis functions is attractive due to the absence of a mesh and the ease of collocation methods. The use of radial basis function for the analysis of structures and materials has been previously studied by numerous authors [16–27]. An interesting alternative to the present work was proposed by Xiang et al. [28,29], who employed thin-plate splines to compute free vibrations of laminated plates, to extract the natural frequencies. An interesting new meshless technique (ES-FEM) was recently proposed by Liu and colleagues [30–35]. The technique is based on weak-form formulations, unlike the present paper which is based on strong-forms (RBF collocation). This method seems to be very precise, and free from locking and spurious behavior. Another possible advantage of the ES-FEM is that it needs the imposition of essential boundary conditions only, while the present collocation method needs both essential and natural boundary conditions.

The authors have recently applied the RBF collocation to the static deformations of composite beams and plates [36–38].

In this paper it is investigated for the first time how the Unified Formulation can be combined with radial basis functions to the analysis of thick isotropic and cross-ply laminated plates, using a first-order shear deformation theory and a refined higher-order shear and normal deformation theory. The quality of the present method in predicting static deformations, and free vibrations of thick isotropic and cross-ply laminated plates is compared and discussed with other methods in some numerical examples.

2. Review of the Unified Formulation

In this section Carrera's Unified Formulation [1–5] is briefly reviewed. It is shown how to obtain the fundamental nuclei, which allows the derivation of the equations of motion and boundary conditions, in weak form for the finite element analysis; and in strong form for the present RBF collocation.

2.1. Governing equations and boundary conditions in the framework of Unified Formulation

Although one can use the UF for one-layer, isotropic plate, a multi-layered plate with N_l layers is considered. The Principle of Virtual Displacements (PVD) for the pure-mechanical case reads as

$$\sum_{k=1}^{N_l} \int_{\Omega_k} \int_{A_k} \{\delta \boldsymbol{\varepsilon}_{pG}^k \mathrm{T} \boldsymbol{\sigma}_{pC}^k + \delta \boldsymbol{\varepsilon}_{nG}^k \mathrm{T} \boldsymbol{\sigma}_{nC}^k\} \, \mathrm{d}\Omega_k \, \mathrm{d}z = \sum_{k=1}^{N_l} \delta L_e^k, \tag{1}$$

where Ω_k and A_k are the integration domains in plane (x,y) and z direction, respectively. Here, k indicates the layer and T the transpose of a vector, and δL_e^k is the external work for the kth layer. G means geometrical relations and C constitutive equations.

The steps to obtain the governing equations are:

- Substitution of the geometrical relations (subscript G).
- Substitution of the appropriate constitutive equations (subscript C).
- Introduction of the Unified Formulation.

Stresses and strains are separated into in-plane and normal components, denoted, respectively, by the subscripts p and n. The mechanical strains in the kth layer can be related to the displacement field $\mathbf{u}^k = \{u_x^k, u_y^k, u_z^k\}$ via the geometrical relations:

$$\begin{aligned} \boldsymbol{\varepsilon}_{pG}^k &= [\varepsilon_{xx}, \varepsilon_{yy}, \gamma_{xy}]^{kT} = \mathbf{D}_p^k \mathbf{u}^k, \\ \boldsymbol{\varepsilon}_{nG}^k &= [\gamma_{xz}, \gamma_{yz}, \varepsilon_{zz}]^{kT} = (\mathbf{D}_{np}^k + \mathbf{D}_{nz}^k)\mathbf{u}^k, \end{aligned} \tag{2}$$

wherein the differential operator arrays are defined as follows:

$$\mathbf{D}_p^k=\begin{bmatrix}\partial_x & 0 & 0\\ 0 & \partial_y & 0\\ \partial_y & \partial_x & 0\end{bmatrix},\quad \mathbf{D}_{np}^k=\begin{bmatrix}0 & 0 & \partial_x\\ 0 & 0 & \partial_y\\ 0 & 0 & 0\end{bmatrix},\quad \mathbf{D}_{nz}^k=\begin{bmatrix}\partial_z & 0 & 0\\ 0 & \partial_z & 0\\ 0 & 0 & \partial_z\end{bmatrix}, \tag{3}$$

The 3D constitutive equations are given as

$$\begin{aligned}\boldsymbol{\sigma}_{pC}^k&=\mathbf{C}_{pp}^k\boldsymbol{\varepsilon}_{pG}^k+\mathbf{C}_{pn}^k\boldsymbol{\varepsilon}_{nG}^k,\\ \boldsymbol{\sigma}_{nC}^k&=\mathbf{C}_{np}^k\boldsymbol{\varepsilon}_{pG}^k+\mathbf{C}_{nn}^k\boldsymbol{\varepsilon}_{nG}^k\end{aligned} \tag{4}$$

with

$$\begin{aligned}\mathbf{C}_{pp}^k&=\begin{bmatrix}C_{11} & C_{12} & C_{16}\\ C_{12} & C_{22} & C_{26}\\ C_{16} & C_{26} & C_{66}\end{bmatrix},\quad \mathbf{C}_{pn}^k=\begin{bmatrix}0 & 0 & C_{13}\\ 0 & 0 & C_{23}\\ 0 & 0 & C_{36}\end{bmatrix},\\ \mathbf{C}_{np}^k&=\begin{bmatrix}0 & 0 & 0\\ 0 & 0 & 0\\ C_{13} & C_{23} & C_{36}\end{bmatrix},\quad \mathbf{C}_{nn}^k=\begin{bmatrix}C_{55} & C_{45} & 0\\ C_{45} & C_{44} & 0\\ 0 & 0 & C_{33}\end{bmatrix}.\end{aligned} \tag{5}$$

According to the Unified Formulation by Carrera, the three displacement components u_x, u_y and u_z and their relative variations can be modeled as

$$(u_x,u_y,u_z)=F_\tau(u_{x\tau},u_{y\tau},u_{z\tau}),\quad (\delta u_x,\delta u_y,\delta u_z)=F_s(\delta u_{xs},\delta u_{ys},\delta u_{zs}) \tag{6}$$

with Taylor expansions from first up to fourth-order: $F_0=z^0=1$, $F_1=z^1=z,\ldots,F_N=z^N,\ldots,F_4=z^4$ if an equivalent single layer (ESL) approach is used.

In case of layerwise (LW) models, each layer k of the given multi-layered structure is separately considered:

$$(u_x^k,u_y^k,u_z^k)=F_\tau^k(u_{x\tau}^k,u_{y\tau}^k,u_{z\tau}^k),\quad (\delta u_x^k,\delta u_y^k,\delta u_z^k)=F_s^k(\delta u_{xs}^k,\delta u_{ys}^k,\delta u_{zs}^k), \tag{7}$$

where combinations of Legendre polynomials are employed as thickness functions:

$$F_t=\frac{P_0+P_1}{2},\quad F_b=\frac{P_0-P_1}{2},\quad F_l=P_l-P_{l-2}$$

with

$$\tau,s=t,b,l\quad\text{and}\quad l=2,\ldots,14. \tag{8}$$

Here, t and b indicate the top and bottom values for each layer, P_l are the Legendre polynomials ($P_0=1$, $P_1=\zeta_k$, $P_2=(3\zeta_k^2-1)/2$ and so on) with $\zeta_k=2z^k/h^k$ that is the non-dimensionalized thickness coordinate ranging from -1 to $+1$ in each layer k. z_k is the local coordinate and h_k is the thickness of the kth layer.

The chosen functions have the following interesting properties:

$$\begin{aligned}&\zeta_k=+1:\ F_t=1,\quad F_b=0,\quad F_l=0\quad\text{at the top,}\\ &\zeta_k=-1:\ F_t=0,\quad F_b=1,\quad F_l=0\quad\text{at the bottom.}\end{aligned} \tag{9}$$

It is obvious that for a single layer shell the ESL and LW evaluations coincide. In Figs. 1 and 2 are shown the assembling procedures on layer k for ESL and LW approaches, respectively.

Substituting the geometrical relations, the constitutive equations and the Unified Formulation into the variational statement PVD for the kth layer, one has

$$\begin{aligned}&\int_{\Omega_k}\int_{A_k}[(\mathbf{D}_p^kF_s\delta\mathbf{u}_s^k)^{\mathrm{T}}(\mathbf{C}_{pp}^k\mathbf{D}_p^kF_\tau\mathbf{u}_\tau^k+\mathbf{C}_{pn}^k(\mathbf{D}_{n\Omega}^k+\mathbf{D}_{nz}^k)F_\tau\mathbf{u}_\tau^k)\\ &+((\mathbf{D}_{n\Omega}^k+\mathbf{D}_{nz}^k)F_s\delta\mathbf{u}_s^k)^{\mathrm{T}}(\mathbf{C}_{np}^k\mathbf{D}_p^kF_\tau\mathbf{u}_\tau^k+\mathbf{C}_{nn}^k(\mathbf{D}_{n\Omega}^k+\mathbf{D}_{nz}^k)F_\tau\mathbf{u}_\tau^k)]\,\mathrm{d}\Omega_k\,\mathrm{d}z=\delta L_e^k.\end{aligned} \tag{10}$$

At this point, the formula of integration by parts is applied:

$$\int_{\Omega_k}((\mathbf{D}_\Omega)\delta\mathbf{a}^k)^{\mathrm{T}}\mathbf{a}^k\,\mathrm{d}\Omega_k=-\int_{\Omega_k}\delta\mathbf{a}^{k\mathrm{T}}((\mathbf{D}_\Omega^{\mathrm{T}})\mathbf{a}^k)\,\mathrm{d}\Omega_k+\int_{\Gamma_k}\delta\mathbf{a}^{k\mathrm{T}}((\mathbf{I}_\Omega)\mathbf{a}^k)\,\mathrm{d}\Gamma_k, \tag{11}$$

where $\mathbf{I}_\Omega$ matrix is obtained applying the *Gradient theorem*:

$$\int_\Omega\frac{\partial\psi}{\partial x_i}\,\mathrm{d}\upsilon=\oint_\Gamma n_i\psi\,\mathrm{d}s, \tag{12}$$

n_i being the components of the normal $\hat{n}$ to the boundary along the direction i.

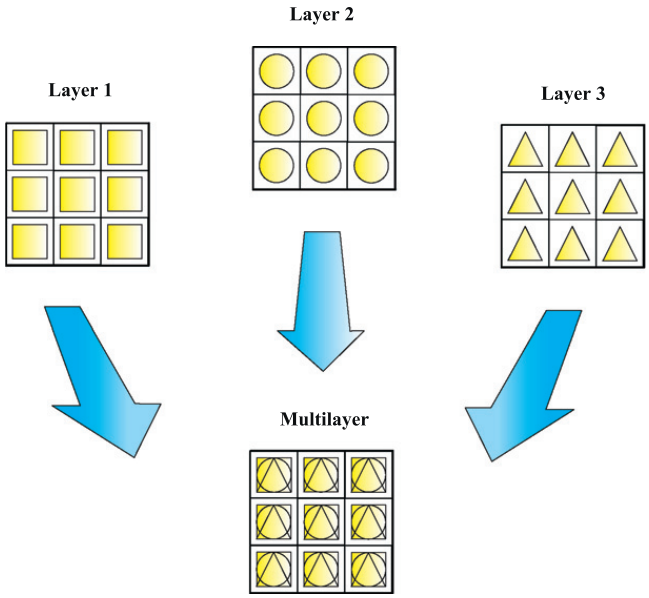

Fig. 1. Assembling procedure for ESL approach.

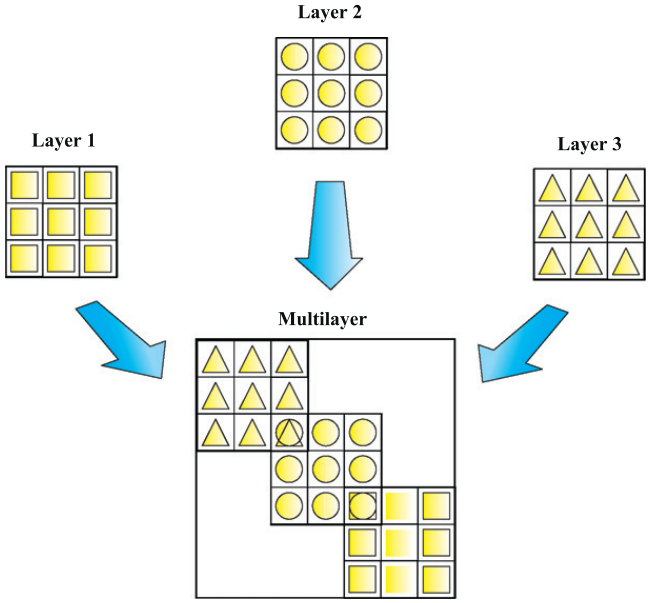

Fig. 2. Assembling procedure for LW approach.

After integration by parts, the governing equations and boundary conditions for the plate in the mechanical case are obtained:

$$\int_{\Omega_k}\int_{A_k}(\delta\mathbf{u}_s^k)^{\mathrm{T}}[((-\mathbf{D}_p^k)^T(\mathbf{C}_{pp}^k(\mathbf{D}_p^k)+\mathbf{C}_{pn}^k(\mathbf{D}_{n\Omega}^k+\mathbf{D}_{nz}^k)$$
$$+(-\mathbf{D}_{n\Omega}^k+\mathbf{D}_{nz}^k)^T(\mathbf{C}_{np}^k(\mathbf{D}_p^k)+\mathbf{C}_{nn}^k(\mathbf{D}_{n\Omega}^k+\mathbf{D}_{nz}^k)))\mathbf{F}_\tau\mathbf{F}_s\mathbf{u}_\tau^k]\,\mathrm{d}x\,\mathrm{d}y\,\mathrm{d}z$$
$$+\int_{\Omega_k}\int_{A_k}(\delta\mathbf{u}_s^k)^{\mathrm{T}}[(\mathbf{I}_p^{kT}(\mathbf{C}_{pp}^k(\mathbf{D}_p^k)+\mathbf{C}_{pn}^k(\mathbf{D}_{n\Omega}^k+\mathbf{D}_{nz}^k))$$
$$+\mathbf{I}_{np}^{kT}(\mathbf{C}_{np}^k(\mathbf{D}_p^k)+\mathbf{C}_{nn}^k(\mathbf{D}_{n\Omega}^k+\mathbf{D}_{nz}^k)))\mathbf{F}_\tau\mathbf{F}_s\mathbf{u}_\tau^k]\,\mathrm{d}x\,\mathrm{d}y\,\mathrm{d}z=\int_{\Omega_k}\delta\mathbf{u}_s^{kT}F_s\mathbf{p}_u^k\,\mathrm{d}\Omega_k, \tag{13}$$

where $\mathbf{I}_p^k$ and $\mathbf{I}_{np}^k$ depend on the boundary geometry:

$$\mathbf{I}_p^k=\begin{bmatrix}n_x & 0 & 0\\ 0 & n_y & 0\\ n_y & n_x & 0\end{bmatrix},\quad \mathbf{I}_{np}^k=\begin{bmatrix}0 & 0 & n_x\\ 0 & 0 & n_y\\ 0 & 0 & 0\end{bmatrix}. \tag{14}$$

The normal to the boundary of domain Ω is

$$\hat{\mathbf{n}} = \begin{bmatrix} n_x \\ n_y \end{bmatrix} = \begin{bmatrix} \cos(\varphi_x) \\ \cos(\varphi_y) \end{bmatrix}, \tag{15}$$

where φ_x and φ_y are the angles between the normal $\hat{n}$ and the directions x and y, respectively.

The governing equations for a multi-layered plate subjected to mechanical loadings are

$$\delta \mathbf{u}_s^k \mathrm{T} : \mathbf{K}_{uu}^{k\tau s} \mathbf{u}_\tau^k = \mathbf{P}_{u\tau}^k, \tag{16}$$

where the fundamental nucleus $\mathbf{K}_{uu}^{k\tau s}$ is obtained as

$$\mathbf{K}_{uu}^{k\tau s} = [(-\mathbf{D}_p^k)^T(\mathbf{C}_{pp}^k(\mathbf{D}_p^k) + \mathbf{C}_{pn}^k(\mathbf{D}_{n\Omega}^k + \mathbf{D}_{nz}^k) + (-\mathbf{D}_{n\Omega}^k + \mathbf{D}_{nz}^k)^T(\mathbf{C}_{np}^k(\mathbf{D}_p^k) + \mathbf{C}_{nn}^k(\mathbf{D}_{n\Omega}^k + \mathbf{D}_{nz}^k))]\mathbf{F}_\tau \mathbf{F}_s \tag{17}$$

and the corresponding Neumann-type boundary conditions on Γ_k are

$$\boldsymbol{\Pi}_d^{k\tau s} \mathbf{u}_\tau^k = \boldsymbol{\Pi}_d^{k\tau s} \overline{\mathbf{u}}_\tau^k, \tag{18}$$

where

$$\boldsymbol{\Pi}_d^{k\tau s} = [\mathbf{I}_p^{kT}(\mathbf{C}_{pp}^k(\mathbf{D}_p^k) + \mathbf{C}_{pn}^k(\mathbf{D}_{n\Omega}^k + \mathbf{D}_{nz}^k)) + \mathbf{I}_{np}^{kT}(\mathbf{C}_{np}^k(\mathbf{D}_p^k) + \mathbf{C}_{nn}^k(\mathbf{D}_{n\Omega}^k + \mathbf{D}_{nz}^k))]\mathbf{F}_\tau \mathbf{F}_s \tag{19}$$

and $\mathbf{P}_{u\tau}^k$ are variationally consistent loads with applied pressure.

2.2. Fundamental nuclei

The fundamental nuclei in explicit form are then obtained as

$$\begin{aligned}
K_{uu_{11}}^{k\tau s} &= (-\partial_x^\tau \partial_x^s C_{11} - \partial_x^\tau \partial_y^s C_{16} + \partial_z^\tau \partial_z^s C_{55} - \partial_y^\tau \partial_x^s C_{16} - \partial_y^\tau \partial_y^s C_{66}) F_\tau F_s, \\
K_{uu_{12}}^{k\tau s} &= (-\partial_x^\tau \partial_y^s C_{12} - \partial_x^\tau \partial_x^s C_{16} + \partial_z^\tau \partial_z^s C_{45} - \partial_y^\tau \partial_y^s C_{26} - \partial_y^\tau \partial_x^s C_{66}) F_\tau F_s, \\
K_{uu_{13}}^{k\tau s} &= (-\partial_x^\tau \partial_z^s C_{13} - \partial_y^\tau \partial_z^s C_{36} + \partial_z^\tau \partial_y^s C_{45} + \partial_z^\tau \partial_x^s C_{55}) F_\tau F_s, \\
K_{uu_{21}}^{k\tau s} &= (-\partial_y^\tau \partial_x^s C_{12} - \partial_y^\tau \partial_y^s C_{26} + \partial_z^\tau \partial_z^s C_{45} - \partial_x^\tau \partial_x^s C_{16} - \partial_x^\tau \partial_y^s C_{66}) F_\tau F_s, \\
K_{uu_{22}}^{k\tau s} &= (-\partial_y^\tau \partial_y^s C_{22} - \partial_y^\tau \partial_x^s C_{26} + \partial_z^\tau \partial_z^s C_{44} - \partial_x^\tau \partial_y^s C_{26} - \partial_x^\tau \partial_x^s C_{66}) F_\tau F_s, \\
K_{uu_{23}}^{k\tau s} &= (-\partial_y^\tau \partial_z^s C_{23} - \partial_x^\tau \partial_z^s C_{36} + \partial_z^\tau \partial_y^s C_{44} + \partial_z^\tau \partial_x^s C_{45}) F_\tau F_s, \\
K_{uu_{31}}^{k\tau s} &= (\partial_z^\tau \partial_x^s C_{13} + \partial_z^\tau \partial_y^s C_{36} - \partial_y^\tau \partial_z^s C_{45} - \partial_x^\tau \partial_z^s C_{55}) F_\tau F_s, \\
K_{uu_{32}}^{k\tau s} &= (\partial_z^\tau \partial_y^s C_{23} + \partial_z^\tau \partial_x^s C_{36} - \partial_y^\tau \partial_z^s C_{44} - \partial_x^\tau \partial_z^s C_{45}) F_\tau F_s, \\
K_{uu_{33}}^{k\tau s} &= (\partial_z^\tau \partial_z^s C_{33} - \partial_y^\tau \partial_y^s C_{44} - \partial_y^\tau \partial_x^s C_{45} - \partial_x^\tau \partial_y^s C_{45} - \partial_x^\tau \partial_x^s C_{55}) F_\tau F_s,
\end{aligned} \tag{20}$$

$$\begin{aligned}
\Pi_{11}^{k\tau s} &= (n_x \partial_x^s C_{11} + n_x \partial_y^s C_{16} + n_y \partial_x^s C_{16} + n_y \partial_y^s C_{66}) F_\tau F_s, \\
\Pi_{12}^{k\tau s} &= (n_x \partial_y^s C_{12} + n_x \partial_x^s C_{16} + n_y \partial_y^s C_{26} + n_y \partial_x^s C_{66}) F_\tau F_s, \\
\Pi_{13}^{k\tau s} &= (n_x \partial_z^s C_{13} + n_y \partial_z^s C_{36}) F_\tau F_s, \\
\Pi_{21}^{k\tau s} &= (n_y \partial_x^s C_{12} + n_y \partial_y^s C_{26} + n_x \partial_x^s C_{16} + n_x \partial_y^s C_{66}) F_\tau F_s, \\
\Pi_{22}^{k\tau s} &= (n_y \partial_y^s C_{22} + n_y \partial_x^s C_{26} + n_x \partial_y^s C_{26} + n_x \partial_x^s C_{66}) F_\tau F_s, \\
\Pi_{23}^{k\tau s} &= (n_y \partial_z^s C_{23} + n_x \partial_z^s C_{36}) F_\tau F_s, \\
\Pi_{31}^{k\tau s} &= (n_y \partial_z^s C_{45} + n_x \partial_z^s C_{55}) F_\tau F_s, \\
\Pi_{32}^{k\tau s} &= (n_y \partial_z^s C_{44} + n_x \partial_z^s C_{45}) F_\tau F_s, \\
\Pi_{33}^{k\tau s} &= (n_y \partial_y^s C_{44} + n_y \partial_x^s C_{45} + n_x \partial_y^s C_{45} + n_x \partial_x^s C_{55}) F_\tau F_s.
\end{aligned} \tag{21}$$

2.3. Dynamic governing equations

The PVD for the dynamic case is expressed as

$$\sum_{k=1}^{N_l}\int_{\Omega_k}\int_{A_k}\{\delta\boldsymbol{\varepsilon}_{pG}^{k}\mathrm{T}\boldsymbol{\sigma}_{pC}^{k}+\delta\boldsymbol{\varepsilon}_{nG}^{k}\mathrm{T}\boldsymbol{\sigma}_{nC}^{k}\}\,\mathrm{d}\Omega_k\,\mathrm{d}z=\sum_{k=1}^{N_l}\int_{\Omega_k}\int_{A_k}\rho^k\delta\mathbf{u}^{kT}\ddot{\mathbf{u}}^k\,\mathrm{d}\Omega_k\,\mathrm{d}z+\sum_{k=1}^{N_l}\delta L_e^k, \tag{22}$$

where ρ^k is the mass density of the kth layer and double dots denote acceleration.

By substituting the geometrical relations, the constitutive equations and the Unified Formulation, we obtain the following governing equations:

$$\delta\mathbf{u}_s^k\mathrm{T}:\mathbf{K}_{uu}^{k\tau s}\mathbf{u}_\tau^k=\mathbf{M}^{k\tau s}\ddot{\mathbf{u}}_\tau^k+\mathbf{P}_{u\tau}^k. \tag{23}$$

In the case of free vibrations one has

$$\delta\mathbf{u}_s^k\mathrm{T}:\ \mathbf{K}_{uu}^{k\tau s}\mathbf{u}_\tau^k=\mathbf{M}^{k\tau s}\ddot{\mathbf{u}}_\tau^k, \tag{24}$$

where $\mathbf{M}^{k\tau s}$ is the fundamental nucleus for the inertial term. The explicit form of that is

$$\begin{aligned}
M_{11}^{k\tau s}&=\rho^k F_\tau F_s,\\
M_{12}^{k\tau s}&=0,\\
M_{13}^{k\tau s}&=0,\\
M_{21}^{k\tau s}&=0,\\
M_{22}^{k\tau s}&=\rho^k F_\tau F_s,\\
M_{23}^{k\tau s}&=0,\\
M_{31}^{k\tau s}&=M_{32}^{k\tau s}=M_{33}^{k\tau s}=\rho^k F_\tau F_s.
\end{aligned} \tag{25}$$

The geometrical and mechanical boundary conditions are the same as the static case.

3. Generation of shear deformation theories

By adequately choosing F_t, F_s, we can generate any type of C^0 shear deformation theory. For example, the FSDT involves the following expansion of displacements:

$$u=u_0+zu_1,\quad v=v_0+zv_1,\quad w=w_0+zw_1. \tag{26}$$

In a typical FSDT, we usually disregard w_1. All we need is to specify F_t=[1 z], and proceed with the adequate integrations in the thickness direction. Note that in this particular theory we use a reduced form of the 3D constitutive stress–strain relations, given that $\sigma_z=0$.

The third-order shear deformation (see Kant [6]) assumes the following displacement field for isotropic or symmetric cross-ply laminated plates:

$$u=zu_1+z^3u_3,\quad v=zv_1+z^3v_3,\quad w=w_0+z^2w_2. \tag{27}$$

To generate the equations of motion, boundary conditions, and so on, we choose F_t=[z z^3] for displacements u,v, and F_t=[1 z^2] for displacement w. We then obtain all terms of the equations of motion by integrating through the thickness direction. For example, the first term of the first equation in (20) becomes

$$-\partial_x^t\partial_x^s\left(\sum_{k=1}^{NL}\int_{z_k}^{z_{k+1}}c_{11}^{(k)}\,\mathrm{d}z\right), \tag{28}$$

where $c_{11}^{(k)}$ is the 11-term of the matrix defined in (5) for layer k, and NL is the number of layers. The terms z_k,z_{k+1} are the global z-coordinate for each layer at its bottom and top surfaces, respectively. Therefore, for the FSDT formulation in the first equation, the first term becomes $A_{11}\partial^2u_0/\partial x^2$, A_{11} being obtained as

$$A_{11}=\sum_{k=1}^{NL}\int_{z_k}^{z_{k+1}}c_{11}^{(k)}\,\mathrm{d}z. \tag{29}$$

The other terms can be obtained in a similar way. It is interesting to note that under this combination of the Unified Formulation and RBF collocation, the collocation code depends only on the choice of F_t, F_s, in order to solve this type of problems. We designed a MATLAB code that just by changing F_t, F_s can analyze static deformations and free vibrations for any type of C^0 shear deformation theory. The equations of motion for the higher-order theory are presented in Appendix.

4. The radial basis function method

4.1. The static problem

Radial basis functions (RBF) approximations are mesh-free numerical schemes that can exploit accurate representations of the boundary, are easy to implement and can be spectrally accurate. In this section the formulation of a global unsymmetrical collocation RBF-based method to compute elliptic operators is presented.

Consider a linear elliptic partial differential operator L and a bounded region Ω in $\mathbb{R}^n$ with some boundary $\partial\Omega$. In the static problems we seek the computation of displacements ($\mathbf{u}$) from the global system of equations

$$L\mathbf{u}=\mathbf{f} \quad \text{in } \Omega, \tag{30}$$

$$L_B\mathbf{u}=\mathbf{g} \quad \text{on } \partial\Omega, \tag{31}$$

where L, L_B are linear operators in the domain and on the boundary, respectively. The right-hand side of (30) and (31) represents the external forces applied on the plate and the boundary conditions applied along the perimeter of the plate, respectively. The PDE problem defined in (30) and (31) will be replaced by a finite problem, defined by an algebraic system of equations, after the radial basis expansions.

4.2. The eigenproblem

The eigenproblem looks for eigenvalues (λ) and eigenvectors ($\mathbf{u}$) that satisfy

$$L\mathbf{u}+\lambda\mathbf{u}=0 \quad \text{in } \Omega, \tag{32}$$

$$L_B\mathbf{u}=0 \quad \text{on } \partial\Omega. \tag{33}$$

As in the static problem, the eigenproblem defined in (32) and (33) is replaced by a finite-dimensional eigenvalue problem, based on RBF approximations.

4.3. Radial basis function approximations

The radial basis function (ϕ) approximation of a function ($\mathbf{u}$) is given by

$$\tilde{\mathbf{u}}(\mathbf{x})=\sum_{i=1}^{N}\alpha_i\phi(\|x-y_i\|_2), \quad \mathbf{x}\in\mathbb{R}^n, \tag{34}$$

where y_i, $i=1,\ldots,N$ is a finite set of distinct points (centers) in $\mathbb{R}^n$. The most common RBFs are

$$\begin{aligned}
\text{Cubic}: &\quad \phi(r)=r^3,\\
\text{Thin plate splines}: &\quad \phi(r)=r^2\log(r),\\
\text{Wendland functions}: &\quad \phi(r)=(1-r)_+^m p(r),\\
\text{Gaussian}: &\quad \phi(r)=\mathrm{e}^{-(cr)^2},\\
\text{Multiquadrics}: &\quad \phi(r)=\sqrt{c^2+r^2},\\
\text{Inverse Multiquadrics}: &\quad \phi(r)=(c^2+r^2)^{-1/2},
\end{aligned}$$

where the Euclidian distance r is real and non-negative and c is a positive shape parameter. Hardy [39] introduced multiquadrics in the analysis of scattered geographical data. In the 1990s Kansa [15] used multiquadrics for the solution of partial differential equations. Considering N distinct interpolations, and knowing $u(x_j)$, $j=1,2,\ldots,N$, we find α_i by the solution of an $N\times N$ linear system

$$\mathbf{A}\underline{\alpha}=\mathbf{u}, \tag{35}$$

where $\mathbf{A}=[\phi(\|x-y_i\|_2)]_{N\times N}$, $\underline{\alpha}=[\alpha_1,\alpha_2,\ldots,\alpha_N]^{\mathrm{T}}$ and $\mathbf{u}=[u(x_1),u(x_2),\ldots,u(x_N)]^T$.

4.4. Solution of the static problem

The solution of a static problem by radial basis functions considers N_I nodes in the domain and N_B nodes on the boundary, with a total number of nodes $N=N_I+N_B$. We denote the sampling points by $x_i\in\Omega$, $i=1,\ldots,N_I$ and $x_i\in\partial\Omega$, $i=N_I+1,\ldots,N$. At the points in the domain we solve the following system of equations:

$$\sum_{i=1}^{N}\alpha_i L\phi(\|x-y_i\|_2)=\mathbf{f}(x_j), \quad j=1,2,\ldots,N_I \tag{36}$$

or

$$L^I\underline{\alpha} = \mathbf{F}, \tag{37}$$

where

$$L^I = [L\phi(\|x-y_i\|_2)]_{N_I\times N}. \tag{38}$$

At the points on the boundary, we impose boundary conditions as

$$\sum_{i=1}^{N} \alpha_i L_B\phi(\|x-y_i\|_2) = \mathbf{g}(x_j), \quad j = N_I+1,\ldots,N \tag{39}$$

or

$$\mathbf{B}\underline{\alpha} = \mathbf{G}. \tag{40}$$

Therefore, we can write a finite-dimensional static problem as

$$\begin{bmatrix} L^I \\ \mathbf{B} \end{bmatrix}\underline{\alpha} = \begin{bmatrix} \mathbf{F} \\ \mathbf{G} \end{bmatrix}. \tag{41}$$

By inverting the system (41), we obtain the vector $\underline{\alpha}$. We then obtain the solution $\mathbf{u}$ using the interpolation equation (34). To keep the collocation matrix as a square matrix, we have used the same number of points and centers.

4.5. Solution of the eigenproblem

We consider N_I nodes in the interior of the domain and N_B nodes on the boundary, with $N=N_I+N_B$. We denote interpolation points by $x_i \in \Omega$, $i=1,\ldots,N_I$ and $x_i \in \partial\Omega$, $i=N_I+1,\ldots,N$. At the points in the domain, we define the eigenproblem as

$$\sum_{i=1}^{N} \alpha_i L\phi(\|x-y_i\|_2) = \lambda\tilde{\mathbf{u}}(x_j), \quad j = 1,2,\ldots,N_I \tag{42}$$

or

$$L^I\underline{\alpha} = \lambda\tilde{\mathbf{u}}^I, \tag{43}$$

where

$$L^I = [L\phi(\|x-y_i\|_2)]_{N_I\times N}. \tag{44}$$

At the points on the boundary, we enforce the boundary conditions as

$$\sum_{i=1}^{N} \alpha_i L_B\phi(\|x-y_i\|_2) = 0, \quad j = N_I+1,\ldots,N \tag{45}$$

or

$$\mathbf{B}\underline{\alpha} = 0. \tag{46}$$

We can then write a finite-dimensional problem as a generalized eigenvalue problem

$$\begin{bmatrix} L^I \\ \mathbf{B} \end{bmatrix}\underline{\alpha} = \lambda\begin{bmatrix} \mathbf{A}^I \\ \mathbf{0} \end{bmatrix}\underline{\alpha}, \tag{47}$$

where

$$\mathbf{A}^I = \phi[(\|x_{N_I}-y_j\|_2)]_{N_I\times N}, \quad \mathbf{B} = L_B\phi[(\|x_{N_I+1}-y_j\|_2)]_{N_B\times N}.$$

5. Discretization of the equations of motion and boundary conditions

The radial basis collocation method follows a simple implementation procedure. Taking Eq. (13), we compute

$$\boldsymbol{\alpha} = \begin{bmatrix} L^I \\ \mathbf{B} \end{bmatrix}^{-1}\begin{bmatrix} \mathbf{F} \\ \mathbf{G} \end{bmatrix}. \tag{48}$$

This $\boldsymbol{\alpha}$ vector is then used to obtain solution $\tilde{\mathbf{u}}$, using (7). If derivatives of $\tilde{\mathbf{u}}$ are needed, such derivatives are computed as

$$\frac{\partial\tilde{\mathbf{u}}}{\partial x} = \sum_{j=1}^{N} \alpha_j \frac{\partial\phi_j}{\partial x}, \tag{49}$$

$$\frac{\partial^2 \tilde{\mathbf{u}}}{\partial x^2} = \sum_{j=1}^{N} \alpha_j \frac{\partial^2 \phi_j}{\partial x^2}, \text{ etc.} \tag{50}$$

In the present collocation approach, we need to impose essential and natural boundary conditions. Consider, for example, the condition $w=0$, on a simply supported or clamped edge. We enforce the conditions by interpolating as

$$w = 0 \rightarrow \sum_{j=1}^{N} \alpha_j^W \phi_j = 0. \tag{51}$$

Other boundary conditions are interpolated in a similar way.

For free vibration problems we set the external force to zero, and assume harmonic solution in terms of displacements $u_0,u_1,v_0,v_1,\ldots$. If we consider the present HSDT, then we express

$$u_1 \equiv \theta_x(x,y,t) = \Psi_x(w,y)e^{i\omega t}, \tag{52}$$

$$u_3 \equiv \theta_x^*(x,y,t) = \Psi_x^*(w,y)e^{i\omega t}, \tag{53}$$

$$v_1 \equiv \theta_y(x,y,t) = \Psi_y(w,y)e^{i\omega t}, \tag{54}$$

$$v_3 \equiv \theta_y^*(x,y,t) = \Psi_y^*(w,y)e^{i\omega t}, \tag{55}$$

$$w_0 \equiv w(x,y,t) = W(w,y)e^{i\omega t}, \tag{56}$$

$$w_2 \equiv w^*(x,y,t) = W^*(w,y)e^{i\omega t}, \tag{57}$$

where ω is the frequency of natural vibration. Substituting the harmonic expansion into Eq. (47) in terms of the amplitudes $W,\Psi_x,\Psi_y,W^*,\Psi_x^*,\Psi_y^*$, we may obtain the natural frequencies and vibration modes for the plate problem.

6. Numerical examples

In all the following examples a Chebyshev grid was used. The Wendland function used in all examples is defined as

$$\phi(r) = (1-c\ r)_+^8 (32(c\ r)^3 + 25(c\ r)^2 + 8c\ r + 1), \tag{58}$$

where the shape parameter (c) is obtained by an optimal procedure, as in Ferreira and Fasshauer [40].

6.1. Static problems—isotropic plates

The first example considers the deflections of simply supported and clamped, uniformly loaded square plate ($a/b=1$, $v=0.3$). We consider thin ($h/a=100$) and thick ($h/a=0.5$) plates, using 13×13, 17×17, 21×21, and 25×25 points.

Tables 1 and 2 compare the present results with the Mindlin (FSDT) theory [41] and the analytical higher-order (HSDT) solution by Kant et al. [6,7]. Note that D is the flexural stiffness ($D=Eh^3/(12(1-v^2))$. The FSDT deviates from the present approach for thicker plates. The results show that the present FSDT and HSDT solution presents good convergence characteristics. The present HSDT numerical technique reproduces almost exactly the analytical solution by Kant, for $z=0$.

Table 1
Convergence study for deflections ($\times pa^4/D$) for uniformly loaded square SSSS plate ($v=0.3$).

h/a	Source	13×13 points	17×17	21×21	25×25
0.01	Present FSDT	0.003968	0.004054	0.004061	0.004064
	Present HSDT	0.003950	0.004052	0.004061	0.004063
	Mindlin [41]	0.00406			
0.1	Present FSDT	0.004270	0.004273	0.004273	0.004272
	Present HSDT	0.004245	0.004249	0.004250	0.004249
	Mindlin [41]	0.00427			
0.2	Present FSDT	0.004902	0.004904	0.004904	0.004904
	Present HSDT	0.004806	0.004805	0.004805	0.004804
	Mindlin [41]	0.00490			
0.5	Present FSDT	0.009322	0.009324	0.009325	0.009324
	Present HSDT	0.008521	0.008523	0.008522	0.008522
	Kant [6,7]	0.00853			

The classical plate solution is 0.00406.

Table 2
Convergence study for deflections ($\times pa^4/D$) for uniformly loaded square CCCC plate ($\nu = 0.3$).

h/a	Source	13×13 points	17×17	21×21	25×25
0.01	Present FSDT	0.001127	0.001267	0.001275	0.001266
	Present HSDT	0.001118	0.001261	0.001268	0.001266
	Mindlin [41]	0.00126			
0.1	Present FSDT	0.001503	0.001505	0.001504	0.001504
	Present HSDT	0.001482	0.001487	0.001488	0.001486
	(at $z=h/2$)	0.001501	0.001508	0.001508	0.001506
	Kant [6,7]	0.00156			
0.2	Present FSDT	0.002171	0.002172	0.002172	0.002172
	Present HSDT	0.002111	0.002118	0.002119	0.002119
	(at $z=h/2$)	0.002178	0.002187	0.002184	0.002186
	Kant [6,7]	0.00211			
0.5	Present FSDT	0.006631	0.006632	0.006632	0.006632
	First higher-order theory	0.006083	0.006089	0.006089	0.006088
	(at $z=h/2$)	0.006741	0.006767	0.006764	0.006764
	Kant [6,7]	0.00609			

The classical plate solution is 0.00126.

Table 3
Natural frequencies of a CCCC square Mindlin/Reissner plate with $h/a=0.1$, $\nu = 0.3$.

Mode no.	13×13	17×17	21×21	Rayleigh–Ritz [42]	Liew et al. [43]
Present FSDT					
1	1.5871	1.5870	1.5870	1.5940	1.5582
2	3.0275	3.0272	3.0270	3.0390	3.0182
3	3.0275	3.0272	3.0272	3.0390	3.0182
4	4.2441	4.2427	4.2433	4.2650	4.1711
Present HSDT					
1	1.5944	1.5944	1.5946	1.5940	1.5582
2	3.0385	3.0373	3.0376	3.0390	3.0182
3	3.0385	3.0373	3.0377	3.0390	3.0182
4	4.2559	4.2518	4.2528	4.2650	4.1711

Interesting to note the difference of the transverse displacement for $z=0$ (middle surface) and for $z=h/2$ (top surface). This effect will surely be more pronounced for sandwich structures. As observed in Table 2, there is a slight oscillation in the normalized transverse displacement. It seems to happen only in the FSDT case. One possible reason for this quite small oscillation is the fact that, for each grid considered, the optimal shape parameter is also slightly different, which may affect the results.

6.2. Free vibration problems—isotropic plates

Natural frequencies and vibration modes are presented for square simply supported and clamped isotropic plates ($a/b=1$). The non-dimensional frequency parameters are given as

$$\overline{\omega} = \omega a\sqrt{\rho/G}, \tag{59}$$

where ω is the frequency, a is the side length, ρ is the mass density per unit volume, G is the shear modulus and $G = E/(2(1+\nu))$, E is Young's modulus and ν is Poisson's ratio.

We compute results for an isotropic plate with different boundary conditions. Firstly, two fully clamped (CCCC) Mindlin/Reissner square plates with different thickness-to-side ratios are considered. The plates are clamped at all boundary edges. The first four modes of vibration for both plates are calculated. Two cases of thickness-to-side ratios $h/a=0.01$ and 0.1 are considered. The comparison of frequency parameters with the Rayleigh–Ritz solutions [42] and results by Liew et al. [43], using a reproducing kernel particle approximation, for each plate is listed in Tables 3 and 4. Excellent agreement is obtained even for a small number of nodes. Our solution is closer to Rayleigh–Ritz solutions than that of Liew. Figs. 3 and 4 present the first eight modal shapes of the CCCC plate ($h/a=0.1$), using a 17×17 nodal grid.

Secondly, fully simply supported (SSSS) Mindlin/Reissner square plates with different thickness-to-side ratios are considered. The first four modes of vibration are computed for two cases of thickness-to-side ratios $h/a=0.01$ and 0.1. Results are compared with 3D-elasticity and Mindlin closed-form solutions [44], and results by Liew et al. [43]. Results are listed in Tables 5 and 6 and show excellent agreement with closed-form solutions.

Table 4
Natural frequencies of a CCCC square Mindlin/Reissner plate with h/a=0.01, $\nu = 0.3$.

Mode no.	13×13	17×17	21×21	Rayleigh–Ritz [42]	Liew et al. [43]
Present FSDT					
1	0.1843	0.1753	0.1753	0.1754	0.1743
2	0.3786	0.3574	0.3572	0.3576	0.3576
3	0.3786	0.3575	0.3574	0.3576	0.3576
4	0.5636	0.5278	0.5273	0.5274	0.5240
Present HSDT					
1	0.1787	0.1770	0.1756	0.1754	0.1743
2	0.3542	0.3630	0.3580	0.3576	0.3576
3	0.3542	0.3630	0.3583	0.3576	0.3576
4	0.5257	0.5373	0.5277	0.5274	0.5240

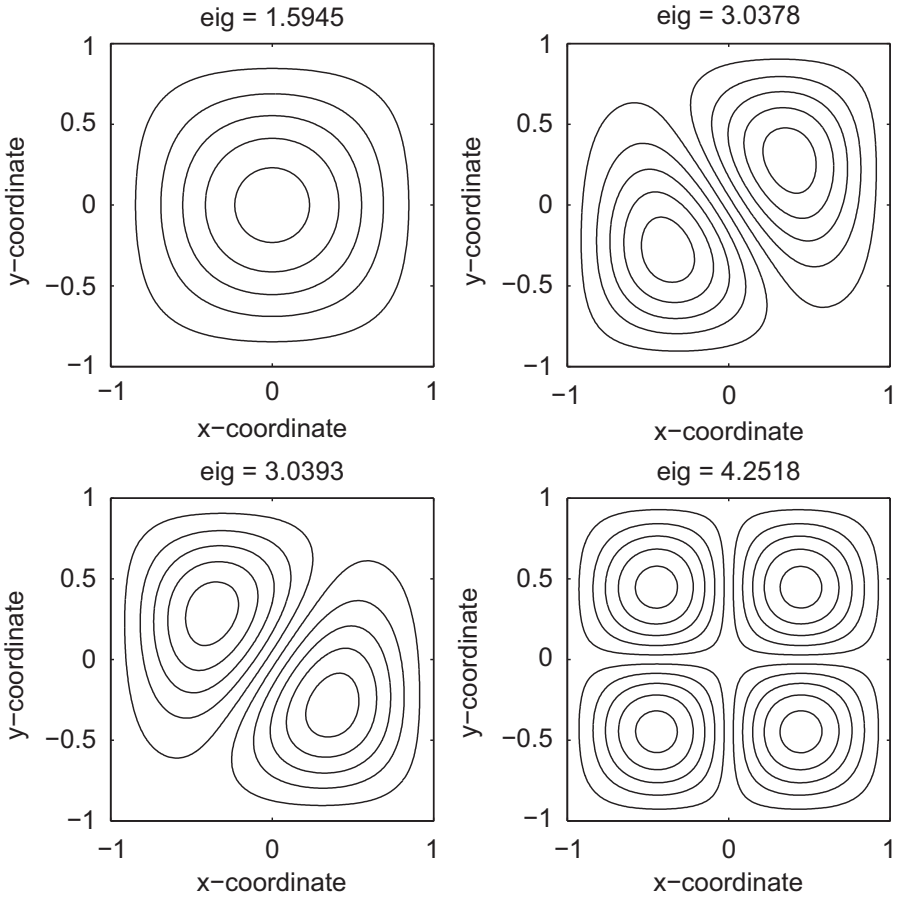

Fig. 3. First four vibrational modes: CCCC, h/a=0.1, grid 17×17.

6.3. Static problems—cross-ply laminated plates

A simply supported square laminated plate of side a and thickness h is composed of four equally layers oriented at [0°/90°/90°/0°]. The plate is subjected to a sinusoidal vertical pressure of the form

$$p_z = P\sin\left(\frac{\pi x}{a}\right)\sin\left(\frac{\pi y}{a}\right)$$

with the origin of the coordinate system located at the lower left corner on the midplane and P the maximum load (at center of plate).

The orthotropic material properties are given by

$$E_1 = 25.0E_2, \quad G_{12} = G_{13} = 0.5E_2, \quad G_{23} = 0.2E_2, \quad \nu_{12} = 0.25.$$

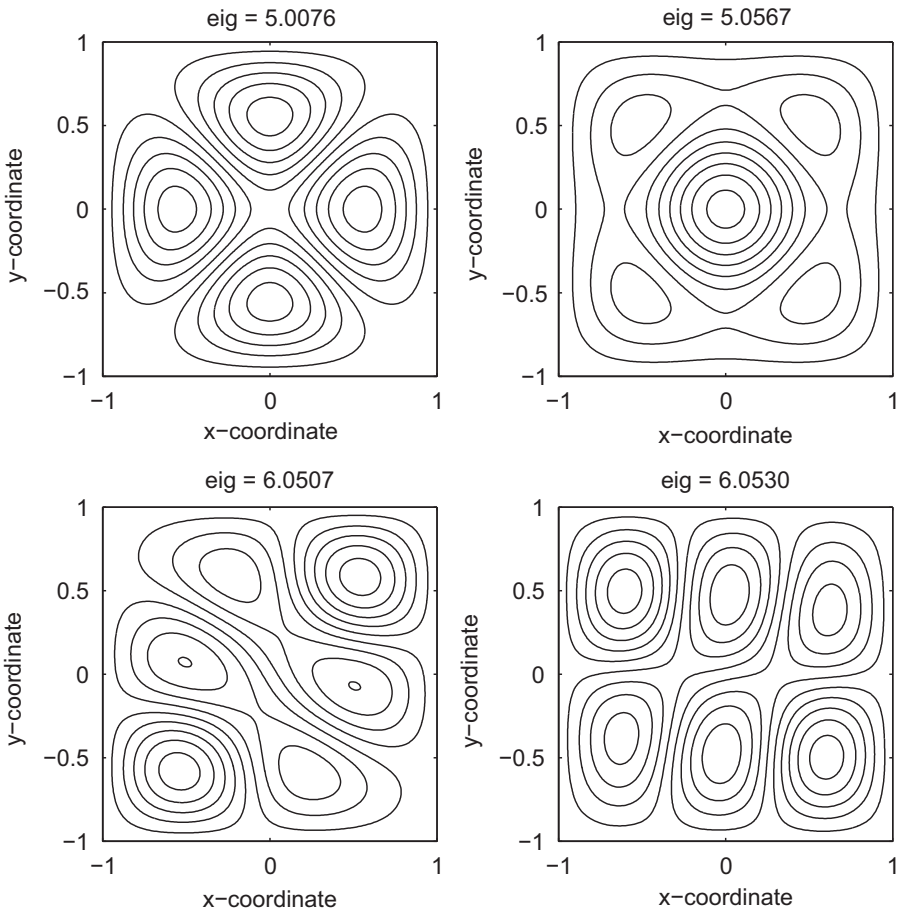

Fig. 4. Fifth to eighth vibrational modes: CCCC, h/a=0.1, grid 17×17.

Table 5
Natural frequencies of a SSSS square Mindlin/Reissner plate with h/a=0.1, $\nu = 0.3$ (*: closed-form solution).

Mode no.	13×13	17×17	21×21	3D*	Mindlin [44]	Liew et al. [43]
Present FSDT						
1	0.9303	0.9303	0.9303	0.932	0.930	0.922
2	2.2195	2.2193	2.2193	2.226	2.219	2.205
3	2.2195	2.2193	2.2193	2.226	2.219	2.205
4	3.1416	3.1416	3.1416	3.421	3.406	3.377
Present HSDT						
1	0.9286	0.9286	0.9286	0.932	0.930	0.922
2	2.2113	2.2111	2.2111	2.226	2.219	2.205
3	2.2113	2.2111	2.2111	2.226	2.219	2.205
4	3.3892	3.3886	3.3886	3.421	3.406	3.377

The in-plane displacements, the transverse displacements, the normal stresses and the in-plane and transverse shear stresses are presented in normalized form as

$$\overline{w} = \frac{10^2 w_{(a/2,a/2,0)} h^3 E_2}{Pa^4}, \quad \overline{\sigma}_{xx} = \frac{\sigma_{xx(a/2,a/2,h/2)} h^2}{Pa^2}, \quad \overline{\sigma}_{yy} = \frac{\sigma_{yy(a/2,a/2,h/4)} h^2}{Pa^2},$$
$$\overline{\tau}_{xz} = \frac{\tau_{xz(0,a/2,0)} h}{Pa}, \quad \overline{\tau}_{xy} = \frac{\tau_{xy(0,0,h/2)} h^2}{Pa^2}.$$

In Table 7 we present results for the present FSDT, and in Table 8 for the present HSDT, using 11×11 up to 21×21 points. We compare results with higher-order solutions by Akhras [45], and Reddy [46], FSDT solutions by Reddy and Chao [47], and an exact solution by Pagano [48]. We also compare the results with authors using RBFs with Reddy's theory [38], and a layerwise theory [49]. As expected both present FSDT and HSDT results are very good for thinner plates, while for

Table 6
Natural frequencies of a SSSS square Mindlin/Reissner plate with h/a=0.01, $\nu = 0.3$.

Mode no.	13×13	17×17	21×21	Mindlin [44]	Liew et al. [43]
Present FSDT					
1	0.0965	0.0963	0.0963	0.0963	0.0961
2	0.2417	0.2407	0.2405	0.2406	0.2419
3	0.2417	0.2407	0.2407	0.2406	0.2419
4	0.3883	0.3851	0.3848	0.3848	0.3860
Present HSDT					
1	0.0965	0.0963	0.0963	0.0963	0.0961
2	0.2416	0.2407	0.2405	0.2406	0.2419
3	0.2416	0.2407	0.2406	0.2406	0.2419
4	0.3885	0.3851	0.3847	0.3848	0.3860

Table 7
$[0^\circ/90^\circ/90^\circ/0^\circ]$ square laminated plate under sinusoidal load-FSDT formulation ($\varepsilon_z = 0$).

$\frac{a}{h}$	Method	$\overline{w}$	$\overline{\sigma}_{xx}$	$\overline{\sigma}_{yy}$	$\overline{\tau}_{zx}$	$\overline{\tau}_{xy}$
4	HSDT Finite Strip method [45]	1.8939	0.6806	0.6463	0.2109	0.0450
	HSDT [46]	1.8937	0.6651	0.6322	0.2064	0.0440
	FSDT [47]	1.7100	0.4059	0.5765	0.1398	0.0308
	Elasticity [48]	1.954	0.720	0.666	0.270	0.0467
	Ferreira et al. [38] (N=21)	1.8864	0.6659	0.6313	0.1352	0.0433
	Ferreira (layerwise) [49] (N=21)	1.9075	0.6432	0.6228	0.2166	0.0441
	Present (11×11 grid)	1.7095	0.4057	0.5762	0.2576	0.0308
	Present (13×13 grid)	1.7095	0.4059	0.5765	0.2675	0.0308
	Present (17×17 grid)	1.7095	0.4059	0.5764	0.2777	0.0308
	Present (21×21 grid)	1.7095	0.4059	0.5764	0.2825	0.0308
10	HSDT Finite Strip method [45]	0.7149	0.5589	0.3974	0.2697	0.0273
	HSDT [46]	0.7147	0.5456	0.3888	0.2640	0.0268
	FSDT [47]	0.6628	0.4989	0.3615	0.1667	0.0241
	Elasticity [48]	0.743	0.559	0.403	0.301	0.0276
	Ferreira et al. [38] (N=21)	0.7153	0.5466	0.4383	0.3347	0.0267
	Ferreira (layerwise) [49] (N=21)	0.7309	0.5496	0.3956	0.2888	0.0273
	Present (11×11 grid)	0.6626	0.4986	0.3614	0.3070	0.0241
	Present (13×13 grid)	0.6627	0.4989	0.3614	0.3188	0.0241
	Present (17×17 grid)	0.6627	0.4989	0.3614	0.3309	0.0241
	Present (21×21 grid)	0.6627	0.4989	0.3614	0.3367	0.0241
100	HSDT Finite Strip method [45]	0.4343	0.5507	0.2769	0.2948	0.0217
	HSDT [46]	0.4343	0.5387	0.2708	0.2897	0.0213
	FSDT [47]	0.4337	0.5382	0.2705	0.1780	0.0213
	Elasticity [48]	0.4347	0.539	0.271	0.339	0.0214
	Ferreira et al. [38] (N=21)	0.4365	0.5413	0.3359	0.4106	0.0215
	Ferreira (layerwise) [49] (N=21)	0.4374	0.5420	0.2697	0.3232	0.0216
	Present (11×11 grid)	0.4325	0.5381	0.2687	0.3291	0.0212
	Present (13×13 grid)	0.4335	0.5378	0.2710	0.3411	0.0213
	Present (17×17 grid)	0.4337	0.5382	0.2705	0.3535	0.0213
	Present (21×21 grid)	0.4337	0.5382	0.2705	0.3596	0.0213

thicker plates, only the HSDT can accurately predict the deflections. Both methods produce highly accurate normal stresses and transverse shear stresses.

6.4. Free vibration problems—cross-ply laminated plates

Unless otherwise stated, all layers of the laminate are assumed to be of the same thickness, density and made of the same linearly elastic composite material. The following material parameters of a layer are used:

$$\frac{E_1}{E_2} = 10,20,30 \text{ or } 40, \quad G_{12} = G_{13} = 0.6E_2, \quad G_3 = 0.5E_2, \quad \nu_{12} = 0.25.$$

The subscripts 1 and 2 denote the directions normal and transverse to the fiber direction in a lamina, which may be oriented at an angle to the plate axes. The ply angle of each layer is measured from the global x-axis to the fiber direction. For the FSDT, we use a shear correction factor $k = \pi^2/12$, as proposed in [50].

Table 8
$[0^\circ/90^\circ/90^\circ/0^\circ]$ square laminated plate under sinusoidal load-HSDT formulation ($\varepsilon_z \neq 0$).

$\frac{a}{h}$	Method	$\overline{w}$	$\overline{\sigma}_{xx}$	$\overline{\sigma}_{yy}$	$\overline{\tau}_{zx}$	$\overline{\tau}_{xy}$
4	HSDT Finite Strip method [45]	1.8939	0.6806	0.6463	0.2109	0.0450
	HSDT [46]	1.8937	0.6651	0.6322	0.2064	0.0440
	FSDT [47]	1.7100	0.4059	0.5765	0.1398	0.0308
	Elasticity [48]	1.954	0.720	0.666	0.270	0.0467
	Ferreira et al. [38] (N=21)	1.8864	0.6659	0.6313	0.1352	0.0433
	Ferreira (layerwise) [49] (N=21)	1.9075	0.6432	0.6228	0.2166	0.0441
	Present (11×11 grid)	1.8843	0.7161	0.6328	0.1896	0.0462
	Present (13×13 grid)	1.8843	0.7163	0.6331	0.1969	0.0462
	Present (17×17 grid)	1.8844	0.7163	0.6330	0.2043	0.0462
	Present (21×21 grid)	1.8844	0.7163	0.6330	0.2079	0.0462
10	HSDT Finite Strip method [45]	0.7149	0.5589	0.3974	0.2697	0.0273
	HSDT [46]	0.7147	0.5456	0.3888	0.2640	0.0268
	FSDT [47]	0.6628	0.4989	0.3615	0.1667	0.0241
	Elasticity [48]	0.743	0.559	0.403	0.301	0.0276
	Ferreira et al. [38] (N=21)	0.7153	0.5466	0.4383	0.3347	0.0267
	Ferreira (layerwise) [49] (N=21)	0.7309	0.5496	0.3956	0.2888	0.0273
	Present (11×11 grid)	0.7204	0.5606	0.3913	0.2513	0.0273
	Present (13×13 grid)	0.7205	0.5607	0.3913	0.2610	0.0273
	Present (17×17 grid)	0.7205	0.5607	0.3913	0.2709	0.0273
	Present (21×21 grid)	0.7205	0.5607	0.3913	0.2756	0.0273
100	HSDT Finite Strip method [45]	0.4343	0.5507	0.2769	0.2948	0.0217
	HSDT [46]	0.4343	0.5387	0.2708	0.2897	0.0213
	FSDT [47]	0.4337	0.5382	0.2705	0.1780	0.0213
	Elasticity [48]	0.4347	0.539	0.271	0.339	0.0214
	Ferreira et al. [38] (N=21)	0.4365	0.5413	0.3359	0.4106	0.0215
	Ferreira (layerwise) [49] (N=21)	0.4374	0.5420	0.2697	0.3232	0.0216
	Present (11×11 grid)	0.4349	0.5380	0.2686	0.2777	0.0214
	Present (13×13 grid)	0.4361	0.5382	0.2713	0.2886	0.0214
	Present (17×17 grid)	0.4362	0.5385	0.2708	0.3001	0.0214
	Present (21×21 grid)	0.4362	0.5385	0.2707	0.3054	0.0214

Table 9
The normalized fundamental frequency of the simply supported cross-ply laminated square plate $[0^\circ/90^\circ/90^\circ/0^\circ]$ ($\overline{w} = (wa^2/h)\sqrt{\rho/E_2}, h/a = 0.2$).

Method	Grid	E_1/E_2			
		10	20	30	40
Liew [50]		8.2924	9.5613	10.320	10.849
Exact (Reddy, Khdeir) [51,52]		8.2982	9.5671	10.326	10.854
Present FSDT	13×13	8.2983	9.5672	10.3259	10.8541
	17×17	8.2982	9.5671	10.3258	10.8540
	21×21	8.2982	9.5671	10.3258	10.8540
Present HSDT ($\nu_{23} = 0.18$)	13×13	8.3001	9.5413	10.2688	10.7653
	17×17	8.2999	9.5411	10.2687	10.7652
	21×21	8.2999	9.5411	10.2687	10.7652

The example considered is a simply supported square plate of the cross-ply lamination $[0^\circ/90^\circ/90^\circ/\ 0^\circ]$. The thickness and length of the plate are denoted by h and a, respectively. The thickness-to-span ratio h/a=0.2 is employed in the computation. Table 9 lists the fundamental frequency of the simply supported laminate made of various modulus ratios of E_1/E_2. It is found that the results are in very close agreement with the values of [51,52] and the meshfree results of Liew [50] based on the FSDT. The relative errors between the analytical and present solutions are around 0.2 percent when we use a 13×13 grid for E_1/E_2=10 and 0.1 percent when we use a 13×13 grid for E_1/E_2=40.

7. Conclusions

In this paper we presented, for the first time, a study using the radial basis function collocation method to analyze static deformations and free vibrations of thick plates using a first-order shear deformation theory; and a higher-order shear and normal deformation theory of Kant, allowing for transverse normal deformations.

Using the Unified Formulation with the radial basis collocation, all the C^0 plate formulations can be easily discretized by radial basis functions collocation. This has not been done before and this paper serves to fill this gap of knowledge in this

area. Also, the burden of deriving the equations of motion and boundary conditions is eliminated with the present approach. All that is needed is to change one vector F_t that defines the expansion of displacements. The MATLAB code automatically solves the static problem or the free vibration problem, irrespective of the shear deformation theory we use. This represents an enormous flexibility and it can be extended easily to other related problems such as bending stress calculations, flexural vibrations and buckling.

We analyzed square isotropic and cross-ply laminated plates in bending and free vibrations. The present results were compared with existing analytical solutions or competitive finite element solutions and very good agreement was observed in both cases.

The present method is a simple yet powerful alternative to other finite element or meshless methods in the static deformation and free vibration analysis of thin and thick isotropic or laminated plates.

Acknowledgements

The support of Ministério da Ciência Tecnologia e do Ensino superior and Fundo Social Europeu (MCTES and FSE) under programs POPH-QREN are gratefully acknowledged.

Appendix A. Equations of motion—HSDT

The equations of motion for the current higher-order shear deformation theory for a cross-ply plate of constant ρ across the thickness direction are presented next:

$$\delta u_1:\ \sum_{k=1}^{NL}\int_{z_k}^{z_{k+1}} -c_{11}^{(k)}z^2\frac{\partial^2 u_1}{\partial x^2}+c_{55}^{(k)}u_1-c_{66}^{(k)}z^2\frac{\partial^2 u_1}{\partial y^2}-c_{11}^{(k)}z^4\frac{\partial^2 u_3}{\partial x^2}+3z^2c_{55}^{(k)}u_3-c_{66}^{(k)}z^4\frac{\partial^2 u_3}{\partial y^2}$$
$$-c_{12}^{(k)}z^2\frac{\partial^2 v_1}{\partial x\partial y}-c_{66}^{(k)}z^2\frac{\partial^2 v_1}{\partial x\partial y}-c_{12}^{(k)}z^4\frac{\partial^2 v_3}{\partial x\partial y}-c_{66}^{(k)}z^4\frac{\partial^2 v_3}{\partial x\partial y}$$
$$+c_{55}^{(k)}\frac{\partial w_0}{\partial x}+c_{55}^{(k)}z^2\frac{\partial w_0}{\partial x}-c_{13}^{(k)}2z^2\frac{\partial w_2}{\partial x}\,dz=\frac{\rho h^3}{12}\frac{\partial^2 u_1}{\partial t^2}+\frac{\rho h^5}{80}\frac{\partial^2 u_3}{\partial t^2}, \tag{60}$$

$$\delta u_3:\ \sum_{k=1}^{NL}\int_{z_k}^{z_{k+1}} -c_{11}^{(k)}z^4\frac{\partial^2 u_1}{\partial x^2}+c_{55}^{(k)}u_1 3z^2-c_{66}^{(k)}z^4\frac{\partial^2 u_1}{\partial y^2}-c_{11}^{(k)}z^6\frac{\partial^2 u_3}{\partial x^2}+9z^4c_{55}^{(k)}u_3-c_{66}^{(k)}z^6\frac{\partial^2 u_3}{\partial y^2}$$
$$-c_{12}^{(k)}z^4\frac{\partial^2 v_1}{\partial x\partial y}-c_{66}^{(k)}z^4\frac{\partial^2 v_1}{\partial x\partial y}-c_{12}^{(k)}z^6\frac{\partial^2 v_3}{\partial x\partial y}-c_{66}^{(k)}z^6\frac{\partial^2 v_3}{\partial x\partial y}$$
$$+c_{55}^{(k)}\frac{\partial w_0}{\partial x}3z^2+c_{55}^{(k)}3z^4\frac{\partial w_0}{\partial x}-c_{13}^{(k)}2z^4\frac{\partial w_2}{\partial x}\,dz=\frac{\rho h^5}{80}\frac{\partial^2 u_1}{\partial t^2}+\frac{\rho h^7}{448}\frac{\partial^2 u_3}{\partial t^2}, \tag{61}$$

$$\delta v_1:\ \sum_{k=1}^{NL}\int_{z_k}^{z_{k+1}} -c_{12}^{(k)}z^2\frac{\partial^2 u_1}{\partial x\partial y}-c_{66}^{(k)}z^2\frac{\partial^2 u_1}{\partial x\partial y}-c_{12}^{(k)}z^4\frac{\partial^2 u_3}{\partial x\partial y}-c_{66}^{(k)}z^4\frac{\partial^2 u_3}{\partial x\partial y}$$
$$-c_{22}^{(k)}z^2\frac{\partial^2 v_1}{\partial y^2}+c_{44}v_1-c_{66}^{(k)}z^2\frac{\partial^2 v_1}{\partial x^2}-c_{22}^{(k)}z^4\frac{\partial^2 v_3}{\partial y^2}+c_{44}v_3 3z^2-c_{66}^{(k)}z^4\frac{\partial^2 v_3}{\partial x^2}$$
$$+c_{44}^{(k)}\frac{\partial w_0}{\partial y}+c_{44}^{(k)}z^2\frac{\partial w_0}{\partial y}-c_{23}^{(k)}2z^2\frac{\partial w_2}{\partial y}\,dz=\frac{\rho h^3}{12}\frac{\partial^2 v_1}{\partial t^2}+\frac{\rho h^5}{80}\frac{\partial^2 v_3}{\partial t^2}, \tag{62}$$

$$\delta v_3:\ \sum_{k=1}^{NL}\int_{z_k}^{z_{k+1}} -c_{12}^{(k)}z^4\frac{\partial^2 u_1}{\partial x\partial y}-c_{66}^{(k)}z^4\frac{\partial^2 u_1}{\partial x\partial y}-c_{12}^{(k)}z^6\frac{\partial^2 u_3}{\partial x\partial y}-c_{66}^{(k)}z^6\frac{\partial^2 u_3}{\partial x\partial y}$$
$$-c_{22}^{(k)}z^4\frac{\partial^2 v_1}{\partial y^2}+c_{44}v_1 3z^2-c_{66}^{(k)}z^4\frac{\partial^2 v_1}{\partial x^2}-c_{22}^{(k)}z^6\frac{\partial^2 v_3}{\partial y^2}+c_{44}v_3 9z^4-c_{66}^{(k)}z^6\frac{\partial^2 v_3}{\partial x^2}$$
$$+c_{44}^{(k)}\frac{\partial w_0}{\partial y}3z^2+c_{44}^{(k)}3z^4\frac{\partial w_0}{\partial y}-c_{23}^{(k)}2z^4\frac{\partial w_2}{\partial y}\,dz=\frac{\rho h^5}{80}\frac{\partial^2 v_1}{\partial t^2}+\frac{\rho h^7}{448}\frac{\partial^2 v_3}{\partial t^2}, \tag{63}$$

$$\delta w_0:\ \sum_{k=1}^{NL}\int_{z_k}^{z_{k+1}} -c_{55}^{(k)}\frac{\partial u_1}{\partial x}-c_{55}^{(k)}\frac{\partial u_3}{\partial x}3z^2-c_{44}^{(k)}\frac{\partial v_1}{\partial y}-c_{44}^{(k)}\frac{\partial v_3}{\partial y}3z^2$$
$$-c_{44}^{(k)}\frac{\partial^2 w_0}{\partial y^2}-c_{55}^{(k)}\frac{\partial^2 w_0}{\partial x^2}-c_{44}^{(k)}\frac{\partial^2 w_2}{\partial y^2}z^2-c_{55}^{(k)}\frac{\partial^2 w_0}{\partial x^2}z^2dz+q=\rho h\frac{\partial^2 w_0}{\partial t^2}+\frac{\rho h^3}{12}\frac{\partial^2 w_2}{\partial t^2}, \tag{64}$$

$$\delta w_2:\ \sum_{k=1}^{NL}\int_{z_k}^{z_{k+1}} -c_{55}^{(k)}\frac{\partial u_1}{\partial x}z^2-c_{55}^{(k)}\frac{\partial u_3}{\partial x}3z^4-c_{44}^{(k)}\frac{\partial v_1}{\partial y}-c_{44}^{(k)}\frac{\partial v_3}{\partial y}3z^4$$

$$-c_{44}^{(k)}\frac{\partial^2 w_0}{\partial y^2}z^2-c_{55}^{(k)}\frac{\partial^2 w_0}{\partial x^2}z^2-c_{44}^{(k)}\frac{\partial^2 w_2}{\partial y^2}z^4-c_{55}^{(k)}\frac{\partial^2 w_0}{\partial x^2}z^4+c_{33}w_2 4z^2\,\mathrm{d}z$$

$$+c_{13}^{(k)}2z^2\frac{\partial u_1}{\partial x}+c_{13}^{(k)}2z^4\frac{\partial u_3}{\partial x}+c_{23}^{(k)}2z^2\frac{\partial v_1}{\partial y}+c_{23}^{(k)}2z^4\frac{\partial v_3}{\partial y}+qh^2/4=\frac{\rho h^3}{12}\frac{\partial^2 w_0}{\partial t^2}+\frac{\rho h^5}{80}\frac{\partial^2 w_2}{\partial t^2} \tag{65}$$

q being the external load.

References

[1] E. Carrera, C^0 Reissner–Mindlin multilayered plate elements including zig-zag and interlaminar stress continuity, *International Journal of Numerical Methods in Engineering* 39 (1996) 1797–1820.
[2] E. Carrera, B. Kroplin, Zig-zag and interlaminar equilibria effects in large deflection and post-buckling analysis of multilayered plates, *Mechanics of Composite Materials and Structures* 4 (1997) 69–94.
[3] E. Carrera, Evaluation of layer-wise mixed theories for laminated plate analysis, *AIAA Journal* (36) (1998) 830–839.
[4] E. Carrera, Historical review of zig-zag theories for multilayered plates and shells, *Applied Mechanics Reviews* (56) (2003) 287–308.
[5] E. Carrera, Developments, ideas, and evaluations based upon Reissner's mixed variational theorem in the modelling of multilayered plates and shells, *Applied Mechanics Reviews* 54 (2001) 301–329.
[6] T. Kant, Numerical analysis of thick plates, *Computer Methods in Applied Mechanics and Engineering* 31 (1982) 1–18.
[7] T. Kant, D.R.J. Owen, O.C. Zienkiewicz, A refined higher-order C^0 plate element, *Computers and Structures* 15 (2) (1982) 177–183.
[8] K.H. Lo, R.M. Christensen, E.M. Wu, A high-order theory of plate deformation, part 1: homogeneous plates, *Journal of Applied Mechanics* 44 (7) (1977) 663–668.
[9] K.H. Lo, R.M. Christensen, E.M. Wu, A high-order theory of plate deformation, part 2: laminated plates, *Journal of Applied Mechanics* 44 (4) (1977) 669–676.
[10] B.N. Pandya, T. Kant, Higher-order shear deformable theories for flexure of sandwich plates-finite element evaluations, *International Journal of Solids and Structures* 24 (1988) 419–451.
[11] R.C. Batra, S. Vidoli, Higher order piezoelectric plate theory derived from a three-dimensional variational principle, *AIAA Journal* 40 (2002) 91–104.
[12] L. Librescu, A.A. Khdeir, J.N. Reddy, A comprehensive analysis of the state of stress of elastic anisotropic flat plates using refined theories, *Acta Mechanica* 70 (1987) 57–81.
[13] J.N. Reddy, *Mechanics of Laminated Composite Plates*, CRC Press, New York, 1997.
[14] L. Fiedler, F. Vestroni, W. Lacarbonara, A generalized higher-order theory for multi-layered, shear-deformable composite plates, *Acta Mechanica* 209 (2010) 85–98.
[15] E.J. Kansa, Multiquadrics—a scattered data approximation scheme with applications to computational fluid dynamics. i: surface approximations and partial derivative estimates, *Computers and Mathematics with Applications* 19 (8/9) (1990) 127–145.
[16] Y.C. Hon, M.W. Lu, W.M. Xue, Y.M. Zhu, Multiquadric method for the numerical solution of byphasic mixture model, *Applied Mathematics and Computation* 88 (1997) 153–175.
[17] Y.C. Hon, K.F. Cheung, X.Z. Mao, E.J. Kansa, A multiquadric solution for the shallow water equation, *ASCE Journal of Hydraulic Engineering* 125 (5) (1999) 524–533.
[18] J.G. Wang, G.R. Liu, P. Lin, Numerical analysis of Biot's consolidation process by radial point interpolation method, *International Journal of Solids and Structures* 39 (6) (2002) 1557–1573.
[19] G.R. Liu, Y.T. Gu, A local radial point interpolation method (LRPIM) for free vibration analyses of 2-d solids, *Journal of Sound and Vibration* 246 (1) (2001) 29–46.
[20] G.R. Liu, J.G. Wang, A point interpolation meshless method based on radial basis functions, *International Journal for Numerical Methods in Engineering* 54 (2002) 1623–1648.
[21] J.G. Wang, G.R. Liu, On the optimal shape parameters of radial basis functions used for 2-d meshless methods, *Computer Methods in Applied Mechanics and Engineering* 191 (2002) 2611–2630.
[22] X.L. Chen, G.R. Liu, S.P. Lim, An element free Galerkin method for the free vibration analysis of composite laminates of complicated shape, *Composite Structures* 59 (2003) 279–289.
[23] K.Y. Dai, G.R. Liu, S.P. Lim, X.L. Chen, An element free Galerkin method for static and free vibration analysis of shear-deformable laminated composite plates, *Journal of Sound and Vibration* 269 (2004) 633–652.
[24] G.R. Liu, X.L. Chen, Buckling of symmetrically laminated composite plates using the element-free Galerkin method, *International Journal of Structural Stability and Dynamics* 2 (2002) 281–294.
[25] K.M. Liew, X.L. Chen, J.N. Reddy, Mesh-free radial basis function method for buckling analysis of non-uniformity loaded arbitrarily shaped shear deformable plates, *Computer Methods in Applied Mechanics and Engineering* 193 (2004) 205–225.
[26] Y.Q. Huang, Q.S. Li, Bending and buckling analysis of antisymmetric laminates using the moving least square differential quadrature method, *Computer Methods in Applied Mechanics and Engineering* 193 (2004) 3471–3492.
[27] L. Liu, G.R. Liu, V.C.B. Tan, Element free method for static and free vibration analysis of spatial thin shell structures, *Computer Methods in Applied Mechanics and Engineering* 191 (2002) 5923–5942.
[28] S. Xiang, K.M. Wang, Y.T. Ai, Y.D. Sha, H. Shi, Analysis of isotropic, sandwich and laminated plates by a meshless method and various shear deformation theories, *Composite Structures* 91 (1) (2009) 31–37.
[29] S. Xiang, H. Shi, K.M. Wang, Y.T. Ai, Y.D. Sha, Thin plate spline radial basis functions for vibration analysis of clamped laminated composite plates, *European Journal of Mechanics A/Solids* 29 (2010) 844–850.
[30] G.R. Liu, T. Nguyen Thoi, *Smoothed Finite Element Method*, CRC Press, Boca Raton, USA, 2010.
[31] G.R. Liu, T. Nguyen-Thoi, K.Y. Lam, An edge-based smoothed finite element method (ES-FEM) for static, free and forced vibration analyses in solids, *Journal of Sound and Vibration* 320 (2009) 1100–1130.
[32] H. Nguyen-Xuan, G.R. Liu, C. Thai-Hoang, T. Nguyen-Thoi, An edge-based smoothed finite element method with stabilized discrete shear gap technique for analysis of Reissner–Mindlin plates, *Computer Methods in Applied Mechanics and Engineering* 199 (2009) 471–489.
[33] H. Nguyen-Xuan, G.R. Liu, T. Nguyen-Thoi, C. Nguyen-Tran, An edge-based smoothed finite element method for analysis of two-dimensional piezoelectric structures, *Smart Materials and Structures* 18 (6) (2009) 065015.
[34] T. Nguyen-Thoi, G.R. Liu, H.C. Vu-Do, H. Nguyen-Xuan, An edge-based smoothed finite element method (ES-FEM) for visco-elastoplastic analyses of 2d solids using triangular mesh, *Computational Mechanics* 45 (2009) 23–44.
[35] T. Nguyen-Thoi, G.R Liu, H. Nguyen-Xuan, An n-sided polygonal edge-based smoothed finite element method (NES-FEM) for solid mechanics. *International Journal for Numerical Methods in Biomedical Engineering* (2010) DOI:10.1002/cnm.1375.
[36] A.J.M. Ferreira, A formulation of the multiquadric radial basis function method for the analysis of laminated composite plates, *Composite Structures* 59 (2003) 385–392.
[37] A.J.M. Ferreira, Thick composite beam analysis using a global meshless approximation based on radial basis functions, *Mechanics of Advanced Materials and Structures* 10 (2003) 271–284.

[38] A.J.M. Ferreira, C.M.C. Roque, P.A.L.S. Martins, Analysis of composite plates using higher-order shear deformation theory and a finite point formulation based on the multiquadric radial basis function method, *Composites: Part B* 34 (2003) 627–636.
[39] R.L. Hardy, Multiquadric equations of topography and other irregular surfaces, *Geophysical Research* 176 (1971) 1905–1915.
[40] A.J.M. Ferreira, G.E. Fasshauer, Computation of natural frequencies of shear deformable beams and plates by a RBF-pseudospectral method, *Computer Methods in Applied Mechanics and Engineering* 196 (2006) 134–146.
[41] R.D. Mindlin, Influence of rotary inertia and shear in flexural motions of isotropic elastic plates, *Journal of Applied mechanics* 18 (1951) 31–38.
[42] D.J. Dawe, O.L. Roufaeil, Rayleigh–Ritz vibration analysis of Mindlin plates, *Journal of Sound and Vibration* 69 (3) (1980) 345–359.
[43] K.M. Liew, J. Wang, T.Y. Ng, M.J. Tan, Free vibration and buckling analyses of shear-deformable plates based on FSDT meshfree method, *Journal of Sound and Vibration* 276 (2004) 997–1017.
[44] E. Hinton, *Numerical Methods and Software for Dynamic Analysis of Plates and Shells*, Pineridge Press, 1988.
[45] G. Akhras, M.S. Cheung, W. Li, Finite strip analysis for anisotropic laminated composite plates using higher-order deformation theory, *Computers & Structures* 52 (3) (1994) 471–477.
[46] J.N. Reddy, A simple higher-order theory for laminated composite plates, *Journal of Applied Mechanics* 51 (1984) 745–752.
[47] J.N. Reddy, W.C. Chao, A comparison of closed-form and finite-element solutions of thick laminated anisotropic rectangular plates, *Nuclear Engineering and Design* 64 (1981) 153–167.
[48] N.J. Pagano, Exact solutions for rectangular bidirectional composites and sandwich plates, *Journal of Composite Materials* 4 (1970) 20–34.
[49] A.J.M. Ferreira, Analysis of composite plates using a layerwise deformation theory and multiquadrics discretization, *Mechanics of Advanced Materials and Structures* 12 (2) (2005) 99–112.
[50] K.M. Liew, Y.Q. Huang, J.N. Reddy, Vibration analysis of symmetrically laminated plates based on FSDT using the moving least squares differential quadrature method, *Computer Methods in Applied Mechanics and Engineering* 192 (2003) 2203–2222.
[51] J.N. Reddy, *Mechanics of Laminated Composite Plates: Theory and Analysis*, CRC Press, Boca Raton, 1997.
[52] A.A. Khdeir, L. Librescu, Analysis of symmetric cross-ply elastic plates using a higher-order theory, part ii: buckling and free vibration, *Composite Structures* 9 (1988) 259–277.